

Complete Coalescence, Partial Bounce and Rebound: Different Regimes Resulting from the Interaction of a Free Falling Drop with a Target Fluid

Yuli D. Chashehkin and Andrey Y. Ilinykh*

Ishlinsky Institute for Problems in Mechanics of the Russian Academy of Sciences, Moscow, 119526, Russia

*Corresponding Author: Andrey Y. Ilinykh. Email: ilynykh@ipmnet.ru

Received: 18 November 2019; Accepted: 08 April 2020

Abstract: The interaction of a falling drop (diluted aqueous solution of ink in various concentrations) with a target fluid (partially degassed tap water) has been tracked by means of high-resolution video recording and photography. The experimental setup has carefully been prepared in order to preserve the axial symmetry of initial conditions. Three regimes of interaction have been identified accordingly (depending on the drop velocity as controlled by the distance of fall): rapid droplet coalescence, rebound with the conservation of the drop volume and shape, and partial coalescence. Previous findings are recovered and confirmed, and enriched with heretofore unseen observations of complex partial coalescence. An extensive set of data is reported to support understanding of the observed dynamics and their repeatability and reproducibility. The overall study has been carried out with the express intent to spur the future development of detailed mathematical models and numerical methods suited for this kind of problems.

Keywords: Drop; coalescence; bounce; spray; transport of matter; miscible fluids

1 Introduction

The first systematic investigation of flow patterns caused by a drop falling on a fluid at rest [1] highly appreciated by contemporaries [2], actively continued and gradually began to make a noticeable effect on the development of general hydrodynamics [3], physics [4], and acoustics [5]. Accessibility of the study object, the variety of picturesque reproducible forms of flows, a growing number of practical applications in the power engineering, aeronautics, Earth sciences, biology, and various technologies in the metallurgical, chemical, and biochemical industries promote saving interest to the problem. The development of the experimental technique (sources of light, photo, and video recorders [6], the use of computer and information technology [7] contributed to the refinement of the properties of the known structural components—a cavity, crown, splash, streamers, capillary waves—in a wide range of parameters as well as confident registration of new, even shorter-lived, and at the same time, stably reproducible components.

In the last years, plane annular jets flying out of the media primary contact region (“ejecta” and “lamina” [8]), regular structures on the contact line of the drop coalescence with a target fluid [9], short capillary waves on the surface of an immersing drop [10], discrete distribution of the drop material in a target fluid—at the bottom of the cavity, the walls of the crown and in vortex loops in the bulk of the fluid [11] were described.



This work is licensed under a Creative Commons Attribution 4.0 International License, which permits unrestricted use, distribution, and reproduction in any medium, provided the original work is properly cited.

Multi-frequency sound packets in water and in the air were registered and their spectral properties were analyzed [5,7].

The investigations of droplet impact on solid surfaces wide spread in technical applications (printing, waterjet cutting, cooling by liquid jets and films [12], dip-pen nanolithography [13], pharmacology). The unsteady internal flow of evaporating droplets under high-temperature environment is of significant interest for cooling processes [14]. In the biochemical application, separation, selection and different mechanisms of manipulation of separated water and oil droplets by the fluidic oscillator were observed in [15], flow patterns in different regions of the circulation-deformation map for a liquid drop being in the electric field were studied [16].

In the case of contact of miscible fluids, the process of spreading of freely fallen drop coalescing with the target medium was initially studied [1,8,10,11]. Later, another type of interaction between the drop and the target fluid was described—an elastic rebound from a fluid at rest or performing vertical oscillations [17]. Observations of multiple rebounds of the drop saving its shape and volume supplemented the hydrodynamic formulation of studied problems by modeling quantum effects—investigation of particle-wave dualism [18]. In the given study, in addition to the well-known processes of fallen drop coalescence [1] or rebound [17], another form of the drop interaction with a target fluid at rest namely partial bounce—partial coalescence with the fast ejection of a smaller droplet—is traced in detail.

The mathematical basis of the experiment performing is the classical system of equations of inhomogeneous fluids mechanics, including the transport equations of matter, momentum, and energy [19], which are not given in the paper for brevity. In accordance with modern recommendations, the calculations of the state equations of fluid are carried out on the basis of the Gibbs potential, taking into account the contribution of surface and chemical energy [20]. Depending on the experimental conditions, the energy exchange between the components of the flows can occur rather slowly in diffusion and dissipative processes, more rapidly with the velocity of running flows, with the group velocity of propagating waves—capillary and sound waves are also observed in droplet flows [4,5,7]. The fastest transfer of energy occurs in domains where direct atomic-molecular processes are developed. As experiments show, the effects of anisotropy of atomic-molecular interactions at the boundaries and high-gradient interfaces make a noticeable effect on the dynamics and structure of the processes at drop immersion [10,11,17]. The multiplicity of energy transfer mechanisms gives room to realize varying modes of interaction of a drop with a target fluid during a single process of total coalescence of the primary drop.

2 General Parameters of the Flow

In the case of identical or similar in composition media, the basic parameters include tabular values of the density of media (air ρ_a , target and drop fluid—water ρ_d , further $\rho_{a,d}$), kinematic $\nu_{a,d}$ and dynamic $\mu_{a,d}$ viscosity, full $\sigma_d^a = 73 \text{ g/s}^2$ and normalized to fluid density $\gamma = \sigma_d^a / \rho_d$ surface tension coefficients, acceleration of gravity g ; as well as the experimental conditions—surface area S^D , volume V^D and equivalent droplet diameter D , drop free falling height H or velocity U at the moment of primary contact. The pressures and temperatures for all media are assumed to be the same: $P_d = P_t = P_a$ and $T_d = T_t = T_a$. Basic parameters determine the spatial and temporal scales of the studied processes.

Spatial linear scales are determined by the intrinsic parameters of the media (capillary-gravitational $\delta_g^\gamma = \sqrt{\gamma/g}$, and dissipative-capillary scales $\delta_\nu^v = v^2/\gamma$, $\delta_\nu^\kappa = \kappa^2/\gamma$), by the velocity of the contacting drop (kinematic $\delta_g^U = U_d^2/g$, capillary $\delta_U^\gamma = \gamma/U^2$, and prandtl scales $\delta_U^v = v/U$ and $\delta_U^\kappa = \kappa/U$). Similarly, some of time scales depend only on the parameters of the problem ($\tau_g^\gamma = \sqrt[4]{\gamma/g^3}$, $\tau_\gamma^\kappa = \kappa^3/\gamma^2$, $\tau_\nu^v = v^3/\gamma^2$), velocity ($\tau_U^d = D/U$, $\tau_g^U = U/g$), or the diameter of the drop ($\tau_\gamma^d = \sqrt{D^3/\gamma}$, $\tau_\kappa^\gamma = \kappa D/\gamma$, $\tau_\nu^\gamma = vD/\gamma$, $\tau_v^D = D^2/v$).

The spatial and temporal scales determine the requirements for the experimental technique: the choice of the size of the observation field, the resolution of the optical recorder, and the exposure time. Scale relations determine traditional dimensionless combinations—the Reynolds $Re = D/\delta_U^v$, Froude $Fr = U^2/gD$, Weber $We_d = D/\delta_U^\gamma$, Bond $Bo = D^2/(\delta_g^\gamma)^2$, Ohnesorge $Oh = \sqrt{\delta_v^v/D}$ numbers, which are commonly used in the analysis of experimental results.

3 Technique of Laboratory Experiment

The evolution of the flow pattern during the immersion of a drop of an alizarin ink aqueous solution (at concentrations of 1:2500 to 1:50), freely fallen into partially degassed tap water with depth $h_l = 1$ and 4 cm, was registered by high-speed video recorder (shooting speed—up to 5000 frames/s) and photcamera. The experiments were performed on the TBP and ESP setups, included in the complex USF “HPC IPMech RAS” [21].

The observation area was illuminated by Optronis MultiLED LED sources using a series of reflective and diffuse screens. The target fluid was placed in crystalline pools with a size of $10 \times 10 \times 5$ cm. Drops of dyed fluid freely fell from the dispenser located above the pool. The angle of sight at the center of the contact region of the drop with the unperturbed surface was from 0° to 65° to the horizontal. The experimental technique is described in more detail in [11].

4 Drop Coalescence at Low Height of Free Falling

In addition to the known modes of the falling drop with the target fluid interaction (continuous coalescence [1,6,11] and elastic rebound [17,18]), a fast partial absorption of drop with ejection of a secondary drop of a smaller size was observed in series of experiments carried out in the range of free fall heights from 1 to 70 cm. The latter type of flow is most clearly visualized at low primary contact velocities. Excerpts from the videogram illustrating the evolution of the flow pattern during free fall of a drop from a low height ($H = 1$ cm) are shown in Fig. 1.

The shape of the drop pinched off from the dispenser is changed under the influence of its own low-frequency oscillations and high-frequency short waves. At contact with the target fluid with a speed of $U = 36$ cm/s, the drop begins to spread actively and forms an invading intrusion with a conical upper part. As a result, a narrow bridge is formed around the contact surface of the coalescing fluids (Fig. 1, $t = 0.6$ ms, time is counted from the moment of initial contact of the lower edge of the drop with the surface of the target fluid).

Capillary waves with the length $0.028 < \lambda < 0.032$ cm propagate from the bridge to the top of the drop remnant. The waves are visualized by a system of dark and gray bands on the residual of the drop in Fig. 1, $t = 6.6$ ms. On the lower convex boundary of the intrusion, individual local inhomogeneities (small vortices) are visible. In this phase, there are no expressed troughs on the free surface, although drop fluid together with the specific momentum and kinetic energy are transferred into the bulk of target fluid.

Quite quickly ($\Delta t = 4.9$ ms), an annular vortex is formed inside the intrusion (Fig. 1, $t = 11.5$ ms, the large R and small r radii of the ring are equal to $R = 0.28$ and $r = 0.065$ cm, respectively). Gradually the vortex ring becomes the main structural component of the flow. The immersion velocity of the lower edge of the vortex ring in the initial period is about $u_r = 23$ cm/s and compatible with the drop contact velocity $U = 36$ cm/s.

With a delay of $\Delta t = 11.5$ ms, which corresponds to the passage of the upper edge of the droplet through the free surface, the cavity begins to be formed in the center of the flow and fast grows. The rate of the cavity depth grows reaches $u_c = 90$ cm/s in the phase of its formation and noticeably exceeds the velocity of immersion of the upper edge of the drop $U = 36$ cm/s. During 8 ms, the cavity reaches a maximum depth of 0.3 cm ($t = 19$ ms). Further, the depth of the cavity begins to decrease, and the width continues

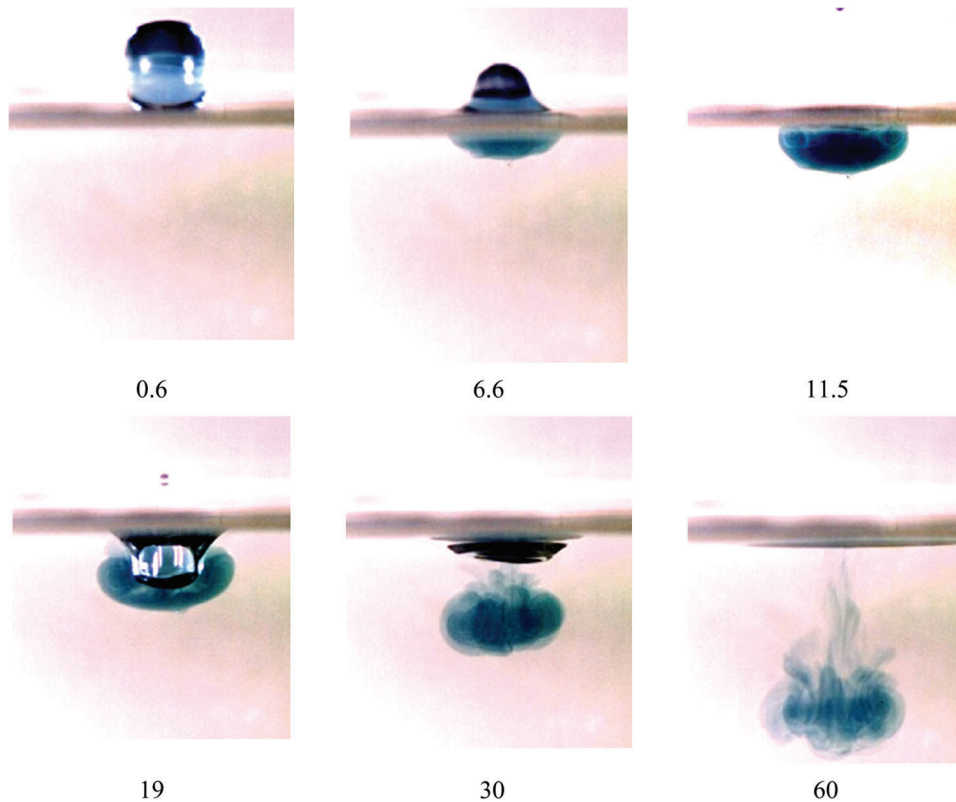


Figure 1: The evolution of the flow pattern at the immersion of an ink solution drop into clean water (concentration 1:1000, $D = 4.3$ cm, $H = 1$ cm, $U = 36$ cm/s, side view), the numbers under the photographs indicate the time in milliseconds

to grow monotonously with a constant velocity of 20 cm/s at the time interval of $\Delta t = 19$ ms. The vortex ring, which is pinched off from the cavity, is contracted a bit: its horizontal size decreases from 0.67 to 0.59 cm. At the same time, its vertical velocity decreases to $u_r = 8$ cm/s.

At the final stage (Fig. 1, $t = 30$ ms), the part of the droplet material spreads over the free surface, the part is transported by the vortex ring into the fluid bulk. The vortex flow loses homogeneity in the azimuthal direction and separates on individual sections, where new, more compact vortices are formed. Vortex loops expand faster than the neighboring parts of the vortex and separate from the main flow, forming a vortex cascade, which was noticed in the first experiments at the end of the 19th century.

The drop material in both the ring itself and in its wake is distributed extremely unevenly. Individual thin colored fibers with an average thickness of about 0.015 cm are separated by shells of a clean target fluid (Fig. 1, $t = 60$ ms).

5 Drop Rebound Regime

A more detailed flow pattern at the immersion of a droplet is shown in Fig. 2. For the resolution of the thin details of the flow, the conditions of the registration were selected where the drop and its reflection from the free surface are presented (Fig. 2, $t = -0.4$ ms).

An immersing drop quickly spreads over the free surface and forms bounded intrusion, with the upper conical boundary rising above the unperturbed surface of the target fluid. A thin, flat circular ring, tilted a slant angle to the horizon, is expanded. Its thickness is less than 0.01 mm (as the ejecta in experiments

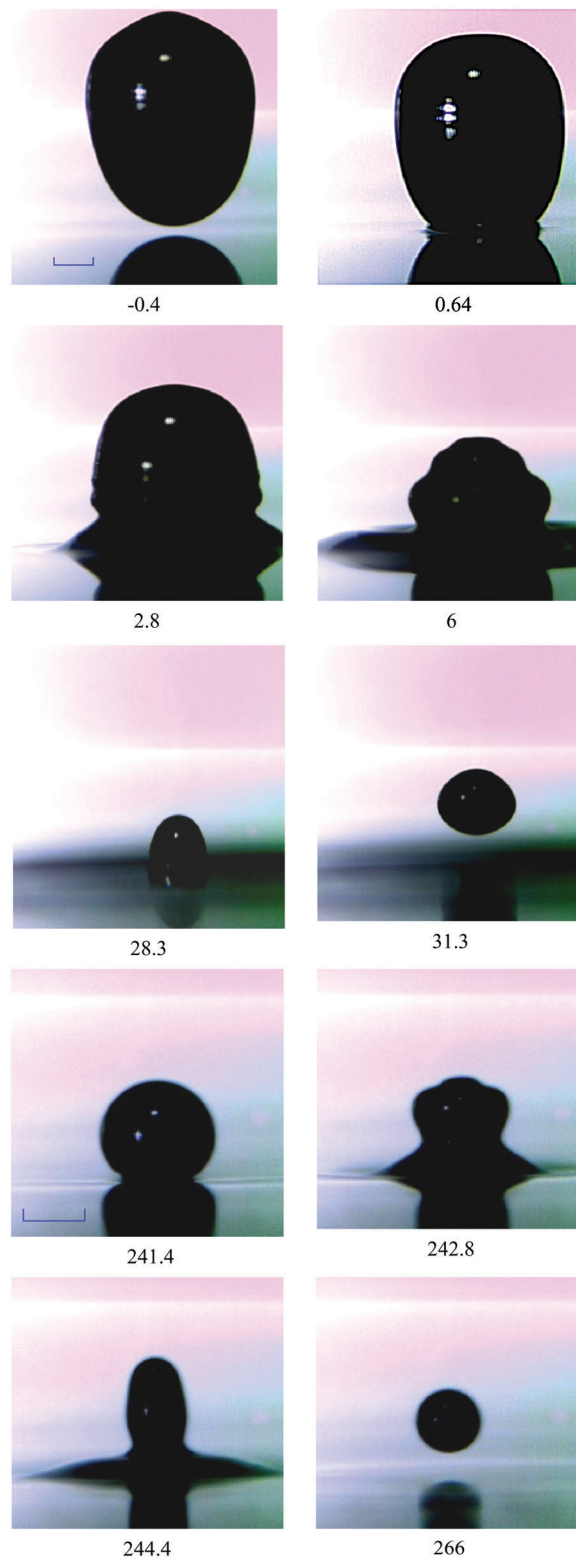


Figure 2: Immersion of the primary drop (concentration of ink dye solution is 1:50, $D = 0.43$ cm, $H = 1$ cm, $U = 36$ cm/s, the length of the marks is 1 mm, side view) and separation of the first ejected drop which starts to eject off the short splash at 244.4 ms, the numbers under the photographs indicate the time in milliseconds

with silicone oil [8]. The ring is formed around a bridge near the contact surface of the immersing fluids and fast evaporates (Fig. 2, $t = 0.64$ ms). Short capillary waves are observed on the surface of the drop residue.

A spreading drop forms a conical colored region with a bridge over the surface; capillary waves from 0.03 to 0.05 cm in length propagate from the bridge to the drop-top (Fig. 2, $t = 2.8$ ms). The diameter of the pedestal at $t = 2.8$ ms reaches 0.62 cm, and the drop residue contracts (the width of the bridge is 0.32 cm). With time, drop residue is immersing, its diameter decreases and a contracting bridge (Fig. 2, $t = 6$ ms) cuts off a part of the drop (Fig. 2, $t = 28.3$ ms), which is ejected into the air (Fig. 2, $t = 31.3$ ms). Here, the first secondary drop with a diameter of $D_1 = 0.2$ cm, which is smaller than the diameter of the primary drop $D = 0.43$ cm, rises to a height of 0.8 cm and then falls onto the perturbed surface of the fluid under the influence of gravity.

The second part of Fig. 2 (from 241.4 to 266 ms) illustrates the process of coalescence of a partially ejected drop with a target fluid which is followed by the formation of a new drop with a smaller diameter. A “hovering drop” separated from the target fluid by a thin air layer has an almost regular shape. The droplet oscillates and moves irregularly in the vertical direction (“droplet dance” on the concave surface of the fluid, Fig. 2, $t = 241.4$ ms). As soon as the air gap is squeezed and the fluids contact, the drop begins to actively invade the target medium and spreads with the formation of a conical pedestal ($t = 242.8$ ms), as in the case of the fall of the primary drop ($t = 2.8$ ms).

In course of time, the height of the pedestal begins to decrease, the diameter continues to increase, drop residue contracts and takes the form of a vertically elongated cylinder with a rounded top (Fig. 2, $t = 244.4$ ms). As the conical pedestal submerges, the contracting annular isthmus completely separates the drop from the target fluid ($t = 250$ ms). The ejected drop at $t = 266$ ms has the correct spherical shape with $D_2 = 1.1$ mm. Further, both elastic rebound and partial absorption of the drop fallen onto the perturbed surface of the target fluid and ejection of a next drop residue were observed. At all, up to 6 cycles of drop elastic rebound and partial bounce took place in experiments.

6 Capillary Waves on Surfaces of the Target Fluid and the Drop

The pattern of perturbations of the target fluid surface by a submerging drop is illustrated by frames of the videogram shown in Fig. 3 (top view, the angle of sight is 65° to the horizon). At the moment of contact, part of the droplet quickly spreads in a thin layer near the fluid surface and forms a colored cone inside the forming ring of diverging annular capillary waves (Fig. 3, $t = 3.6$ ms).

Annular waves are observed both on the unperturbed surface of the fluid ($0.028 < \lambda < 0.13$ cm) and on the surface of the drop ($0.04 < \lambda < 0.1$ cm). In this case, the phase velocities of capillary waves are in the range from 56 to 126 cm/s. From the dispersion relation for capillary waves, the dependence of the phase velocity on the wavelength is $c_{ph} = \sqrt{2\pi\sigma/(\rho\lambda)}$ and the group velocity $c_g = 3c_{ph}/2$ is in the range from 84 to 190 cm/s. The smooth annular band being between the drop and the inner edge of the wave system is due to the dispersion properties of gravitational-capillary waves, with the minimum phase velocity to be equal to the group $c_{ph} = c_g = 23.5$ cm/s [22].

After immersion of the first half of the drop, when the contact line of coalescing fluids begins to move toward the center of the flow, the free surface is sharply deformed. And in the contour of the remainder of the drop and on the boundary of the cavity, angular sections appear (Fig. 3, $t = 6.3$ ms). Their appearance is explained by the action of intense subsurface flows, deforming the boundaries of the structural components of the flow. The intense interaction of flows and capillary waves leads to the formation of closed elongated gas fragments, gradually contracting into ellipsoidal gas bubbles, which can be seen in all the photographs shown in Fig. 3 at $t = 6.3$ ms.

For a long time, the spherical remnant of the droplet with a diameter of 0.09 cm remains at the bottom of the cavity (Fig. 3, $t = 11.7$ ms). Under the action of near-surface flows the cavity, originally having a

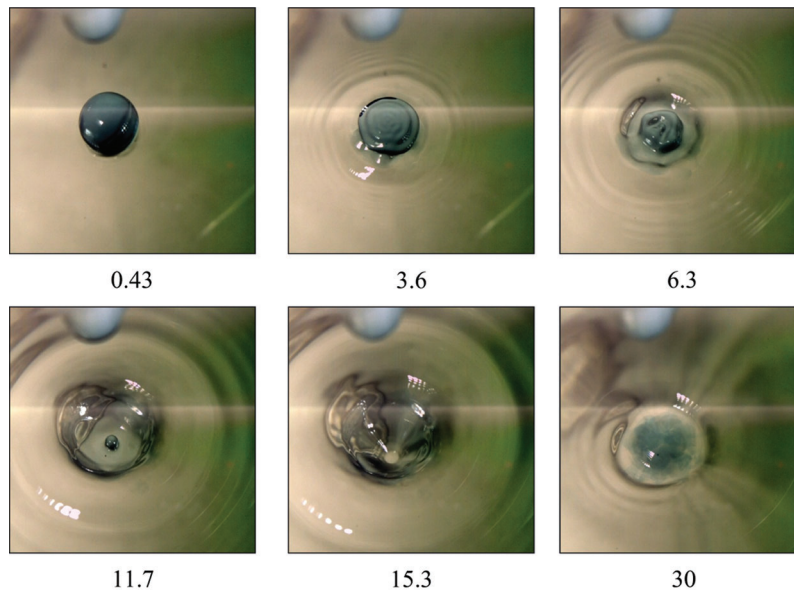


Figure 3: Immersion of an ink solution drop (concentration 1:2500, $D = 0.43$ cm, $U = 36$ cm/s, top view) into clean water, the numbers under the photographs indicate the time in milliseconds

spherical bottom takes a conical shape. A sharp change in the surface curvature is accompanied by the generation of a new group of short capillary waves with a length of 0.08 to 0.16 cm (Fig. 3, $t = 15.3$ ms).

The coalescence of the droplet remnant forms a new conical depression at the bottom of the cavity (Fig. 3, $t = 30$ ms). Two irregular gas fragments are visible on its side surface.

Under the buoyancy forces and surface tension actions, the cavity is collapsed and replaced by a smooth protrusion. Each change in the shape of the cavity is accompanied by an intense movement of its contact line with the rest of the crown and the generation of a new group of capillary waves.

In this experiment, when the oscillations of the falling drop were small, secondary drops were not observed. The vortex system of a colored fluid with a clearly defined central core is separated from the cavity and continues to submerge into the fluid (Fig. 3, $t = 30$ ms).

7 The Sequence of Drop Rebounds and Partial Bounces

The total periodogram of the flow with the formation of secondary drops is shown in Fig. 4 (patterns of the first two drops coalescence are shown in Fig. 2). The distance was measured from the upper edge of the drop to the surface of the undisturbed fluid, which was determined by the position of the primary contact point. The geometric characteristics of the flow are shown in Tab. 1.

The contact of the rapidly falling oscillating droplet with the target fluid is accompanied by partial coalescence and at $t = 30$ ms the secondary drop was ejected with the velocity of $u_1 = 28$ cm/s. The secondary drop also performs decaying volumetric oscillations with a period of $T = 8$ ms.

Under the influence of gravity, the drop begins to fall and at $t = 109$ ms reaches the surface of the target fluid at the center of the primary contact spot. The drop elastically rebounds back to the height of 2.4 mm while preserving its volume, and again falls back onto the free surface at $t = 143$ ms, where it transforms into the “hovering drop” undergoing small oscillations (cycle time flight is $\Delta t = 34$ ms).

At $t = 240$ ms, when the drop again touches the target fluid, a new cycle of partial absorption, the formation of a pedestal and ejection of the residue with the repetition of the details of the process

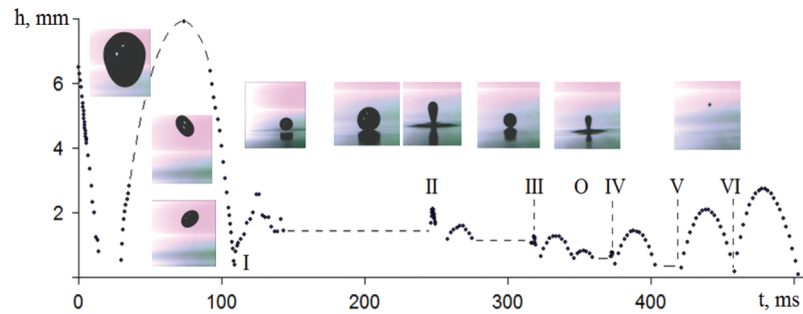


Figure 4: The periodogram of the primary and the sequence of ejected drops motions with durations of coalescence phase, rebound and partial bounce of drops equal I—8 ms, II—5 ms, III—3 ms, IV—2 ms, V—1 ms, VI—0.5 ms

Table 1: Parameters of primary and sequentially ejected drops

N	D_n , mm	ΔT , ms	S_n , mm ²	V_n , mm ³	E_k , nJ	E_σ , nJ	$(E_p/E_\sigma) \cdot 10^2$	$(W_p/W_\sigma) \cdot 10^6$
1	4.3	25	58	42	2700	4200	65	20
2	2	8.3	12.6	4.2	160	900	18	10
3	1.1	3.4	3.8	0.7	3	270	1.3	2
4	0.67	1.6	1.4	0.16	1.5	100	1.5	3
5	0.39	0.7	0.5	0.03	0.35	30	1	4
6	0.23	0.32	0.16	0.006	0.13	12	1	7
7	0.12	0.12	0.05	0.0009	0.03	3	1	10

dynamics start. The duration of the touch-bounce interval of the drop (volume adjustment) is from 8 ms for the primary drop and 5 and 3 for the next two drops.

After that, an elastic rebound, a flight for 20 ms and a new falling on the fluid surface for 40 ms were followed. After the flight and the bounce (O) of the drop residue with a duration of 47 ms, a new phase of falling on the surface with a duration of 12 ms and the last two cycles with a long flight phase and a short tuning time, which is less than 1 ms occur. The trajectory of the secondary drops is vertical or tilted; it randomly changed from number to number and from experiment to experiment. At each contact of the primary and secondary drops with the surface of the fluid, a group of annular capillary waves was generated.

In all phases, durations of the coalescence process and ejection of the drop residue in succession are $\Delta T = 8, 5, 3, 2, 1$, and 0.5 ms, and are significantly less than the residence time on the fluid surface or in free flight, which are $\Delta T = 100, 40, 12$, and 17 ms long. The main parameters of the primary and successively ejected droplets shown in Fig. 4 are presented in Tab. 1.

With each act of partial coalescence, the diameter of the droplet D_n decreases by about 2 times, respectively; the surface S_n decreases by 4 times, and the volume V_n by 7–5 times. The kinetic energy E_k , determined by the velocity and mass of the droplet at the time of departure monotonously decreases its value changes by 5 orders of magnitude. Surface energy E_σ changes by 3 orders of magnitude. The ratios of kinetic to surface energy as well as the ratios of energy densities do not change monotonously, the minimum values are observed in the third cycle.

The values of the main dimensionless parameters are given in Tab. 2. The velocity of the ejected drop also reaches its minimum value in the third cycle, as well as the local Froude and Weber numbers. The Bond number decreases monotonically with increasing droplet number, while the Ohnesorge number grows.

When reproducing the experiments, all modes of the droplet with the target fluid interaction that are total coalescence, ejection of the secondary droplet from the top of the splash, elastic rebound, partial absorption with the rapid ejection of the drop residue were observed for low (2, 3) and high numbers of secondary drops (5, 6).

The character of the interaction of the drop with the target fluid was determined by the dynamic states of the drop, which performed Rayleigh oscillations, and the free surface, along which previously formed short capillary waves propagated. The fine details of the drop fluid motions on the surface of target fluid are also affected by the dust always present in the air, which, as shown by special observations, does not settle uniformly, but forms a net pattern with a high concentration of particles at the cell boundaries.

Table 2: The main dimensionless parameters of droplets of the same sequence

No. of drop	U , cm/s	Re	Fr	We	Bo	Oh $\cdot 10^3$
1	36	1545	7.70	3.1	2.50	1.8
2	28	559	2.17	4.0	0.54	2.6
3	10	110	0.15	0.9	0.16	3.6
4	14	94	0.18	3.0	0.06	4.5
5	15	58	0.12	5.9	0.02	6.0
6	20	46	0.13	17.8	0.007	7.8
7	27	32	0.12	62	0.002	10.8

8 Conclusions

Immersion regimes of a fallen drop (diluted aqueous solution of ink in various concentrations) in a target fluid (partially degassed tap water) were tracked by high-resolution video registration and photography. At high primary contact velocities in the range from 0.35 to 3.7 m/s, the total coalescence regime with a discrete distribution of the droplet substance over the surface of the cavity and crown is well-known. With a decrease of velocity, part of the contacting drop is trapped on the deformed fluid surface. A drop, that sinks at low contact velocity quickly, spreads in the horizontal direction and forms a colored volume with the upper part of the conical shape. Short capillary waves run from the confluence region up the droplet surface. A gradually invading colored liquid produces a vortex ring that includes both interacting fluids in the form of spiral toroidal layers. And only after the colored vortex ring, which retains the inertia of the droplet's motion, separates from the free surface and begins to sink, a cavity begins to form in the target fluid.

In the near-surface layer of the target fluid, fast trickle flows are formed that distort the shape of the contact line of the cavity and crown and deform the cavity, the lower part of which takes a conical shape. Then we observed sequence of flow regimes with ejecting secondary droplets: rapid droplet coalescence, rebound with a saving of the drop volume and shape, hovering of the droplet on the deformed surface of the target fluid and partial coalescence of the droplet with a short splash formation, from the tip of which a smaller droplet was ejected.

At all stages of evolution, each change of the shape of the cavity and crown is accompanied by the generation of a new group of capillary waves that fill the smooth vicinity of the cavity after the entire packet of previously emitted waves run out from the area of observation. Capillary waves are modulated

in an angular variable. The intense near-surface trickle flows cause local overturn of wave crests closing the troughs and the formation of elongated gas fragments of complex shape, gradually transforming into elongated gas bubbles.

In the rapidly changing flow pattern, several repeated processes of immersion of the sequence of droplets ejected from the top of the emerging splashes. Newly returned droplets can hover on the concave surface of the target fluid, rebound with the preservation of the shape and rapidly merge with the distribution of the droplet material along the boundary of the liquid contact area. The droplet residence time in the state associated with the target fluid decreases rapidly with shortening droplet diameter. The velocity of new ejected drops and the duration of the flight phase increase with decreasing droplet size.

The non-monotonous nature of the immersion of a droplet falling at low speed on the surface of a stationary receiving fluid is due to the complex nature of the process of releasing available potential surface energy, the degree of influence of which increases with decreasing droplet size and increases the share of surface energy in the total energy content.

Converted into other forms, the surface energy is stored in a thin double layer in the vicinity of the contact surface of the merging liquids and creates thin surface flows that deform the free surface of the target fluid, contributing to the emergence of a new smaller droplet. The influence of energy in general and the form of equations of state of interacting fluids on the nature of matter transfer, the dynamics and structure of droplet flow need a more in-depth study.

Acknowledgement: The experiments were performed on the TBP and ESP setups, included in the complex of USF “HPC IPMech RAS”.

Funding Statement: This work was supported by the Russian Science Foundation (Project 19-19-00598 “Hydrodynamics and energetics of drops and droplet jets: formation, motion, break-up, interaction with the contact surface”, site: <https://www.rscf.ru/>).

Conflicts of Interest: The authors declare that they have no conflicts of interest to report regarding the present study.

References

1. Worthington, A. (1895). *The splash of the drop, series “The romance of science”*. New York: E. & J. B. Young & Co.
2. Thompson, D. (1992). *On grows and forms*. An abridged edition. Cambridge: CUP.
3. Lenewit, G., Koehler, R., Roesner, G., Schäfer, G. (2005). Regimes of drop morphology in oblique impact on deep fluids. *Journal of Fluid Mechanics*, 543(1), 303–331. DOI 10.1017/S0022112005006476.
4. Prosperetti, A., Oguz, H. (1993). The impact of drops on liquid surfaces and the underwater noise of rain. *Annual Review of Fluid Mechanics*, 25(1), 577–602. DOI 10.1146/annurev.fl.25.010193.003045.
5. Chashechkin, Y., Prokhorov, V. (2015). Fine structure of acoustic signals caused by a drop falling onto the surface of water. *Doklady Physics*, 60(8), 355–359. DOI 10.1134/S1028335815080054.
6. Thoroddsen, S., Etoh, T., Takehara, K. (2008). High-speed imaging of drops and bubbles. *Annual Review of Fluid Mechanics*, 40(1), 257–285. DOI 10.1146/annurev.fluid.40.111406.102215.
7. Chashechkin, Y., Prokhorov, V. (2016). Primary acoustic signal structure during free falling drop collision with a water surface. *Journal of Experimental and Theoretical Physics*, 122(4), 748–758. DOI 10.1134/S1063776116020175.
8. Zhang, L., Toole, J., Fezzaa, K., Deegan, R. (2012). Evolution of the ejecta sheet from the impact of a drop with a deep pool. *Journal of Fluid Mechanics*, 690, 5–15. DOI 10.1017/jfm.2011.396.
9. Li, E., Thoraval, M. J., Marston, J., Thoroddsen, S. (2018). Early azimuthal instability during drop impact. *Journal of Fluid Mechanics*, 848, 821–835. DOI 10.1017/jfm.2018.383.

10. Chashechkin, Y., Ilyinykh, A. (2015). Capillary waves on the surface of the liquid droplets in submerging in a fluid drop. *Doklady Physics*, 60(12), 434–440.
11. Chashechkin, Y., Ilyinykh, A. (2018). Banded structures in the distribution pattern of a drop over the surface of the target fluid. *Doklady Physics*, 63(7), 282–287. DOI 10.1134/S1028335818070066.
12. Kazachkov, I. (2019). On the modeling of non-classical problems involving liquid jets and films and related heat transfer processes. *Fluid Dynamics & Materials Processing*, 15(5), 491–507. DOI 10.32604/fdmp.2019.06477.
13. Zhang, C., Wu, M. (2019). An analysis of the stretching mechanism of a liquid bridge in typical problems of dip-pen nanolithography by using computational fluid dynamics. *Fluid Dynamics & Materials Processing*, 15(4), 459–469. DOI 10.32604/fdmp.2019.08477.
14. Wang, Z., Dong, K., Zhan, S. (2017). Numerical analysis on unsteady internal flow in an evaporating droplet. *Fluid Dynamics & Materials Processing*, 13(4), 221–234.
15. Chekifi, T., Dennai, B., Khelifaoui, R. (2017). Computational investigation of droplets behaviour inside passive microfluidic oscillator. *Fluid Dynamics & Materials Processing*, 13(3), 173–187.
16. Esmaeeli, A., Behjatian, A. (2017). A note on the transient electrohydrodynamics of a liquid drop. *Fluid Dynamics & Materials Processing*, 13(3), 143–153.
17. Couder, Y., Fort, E., Gautier, C., Boudaoud, A. (2005). From bouncing to floating: noncoalescence of drops on a fluid bath. *Physical Review Letters*, 94(17), 321. DOI 10.1103/PhysRevLett.94.177801.
18. Bush, J. (2015). Pilot-wave hydrodynamics. *Annual Review of Fluid Mechanics*, 47(1), 269–292. DOI 10.1146/annurev-fluid-010814-014506.
19. Landau, L., Lifshitz, E. (1987). *Fluid mechanics*. London: Pergamon.
20. Feistel, R. (2018). Thermodynamic properties of seawater, ice and humid air: TEOS-10, before and beyond. *Ocean Sciences*, 14(3), 471–502. DOI 10.5194/os-14-471-2018.
21. USF “HPC IPMech RAS”. (2018). Unique science facility “Hydrophysical complex for modeling of hydrodynamic processes in the environment and their influence on underwater technical objects, as well as the distribution of impurities in the ocean and atmosphere”. <http://www.ipmnet.ru/uniquequip/gfk/#equip>.
22. Whitham, G. B. (1974). *Linear and nonlinear waves*. Chichester: John Wiley & Sons, Ltd.